Iranian Journal of Science and Technology, Transactions of Civil Engineering
https://doi.org/10.1007/s40996-024-01349-1

RESEARCH PAPER

Sustainable and Economic Base Isolators Made by Scrap Tires for Low-rise Buildings in Developing Countries

Arash Akbari Hamed[1] · Mahsa Saeidzadeh[1] · Hesam Bafandeh Nobari[1] · Farid Ostadhasanzadeh Maleky[1]

Received: 30 October 2023 / Accepted: 9 January 2024

Abstract

The use of common seismic bearings poses a significant challenge due to their high cost, limiting their application to structures with a high occupancy importance factor. Consequently, this research aims to introduce innovative and cost-effective base isolators made from discarded tires. These base isolators are particularly suitable for low-rise buildings in developing countries, offering a sustainable solution to mitigate the environmental impact associated with the tire disposal. The study involved the modeling of six different types of these base isolators, with a focus on evaluating their compression and shear behavior through numerical analysis. The results of the study indicate that base isolators featuring bonded rubber layers and vertical steel rods exhibit the most favorable structural performance. Furthermore, the seismic behavior of two-story steel building models, with both fixed-base and base-isolated configurations, was investigated using earthquake accelerograms. The findings demonstrate that the novel base isolator, incorporating bonded rubber layers and vertical steel rods, can effectively reduce the maximum absolute acceleration, maximum interstory drift ratio and max base shear by an average of 47.73%, 51.13% and 59.27%, respectively. Additionally, this base isolator provides a vertical secant stiffness of 55.25 kN/mm and an average effective damping of 0.16. These outcomes highlight the potential of the proposed base isolator design in enhancing the seismic resilience of structures while offering economic benefits.

Keywords Base isolator · Scrap tires · Low-rise buildings · Sustainable · Economic · Developing countries

1 Introduction

To ensure the structural integrity of buildings and safeguard the lives of occupants from natural calamities like severe earthquakes, structural engineers employ various strategies. These include designating specific zones within the building members that act as fuse elements (Hamed and Basim 2020; Saeidzadeh et al. 2022, 2023), as well as incorporating dampers (Akbari Hamed and Mofid 2015, 2017; Hamed et al. 2022; Akbari Hamed and Hashemi 2023; Akbari Hamed et al. 2023) or base isolators. The purpose of these measures is to dissipate seismic energy and minimize its impact on the structure. Additionally, the use of large-deformable base isolators with low shear modulus, as proposed by Kelly (1993a, b); Naeim and Kelly (1999), serves to prevent the transmission of seismic energy into the building. The conventional base isolators that are commonly used include elastomeric bearings (Kelly 1993a, b) and friction-pendulum bearings (Zayas et al. 1989a, b; Zayas et al. 1989a, b). Despite their excellent seismic performance, these isolators are too expensive to be used in rural or low-rise buildings with the lowest occupancy category in developing countries. Therefore, there is a need to introduce economical seismic base isolators that can be used in buildings with low hazard to human life in failure. One effective solution could be the use of alternative rubber materials with low cost, as rubber is the main material used in conventional elastomeric bearings. According to a report by the Tire Industry Project for the World Business Council for Sustainable Development, there are currently 4 billion end-of-life tires in landfills and stockpiles throughout the world, with a generation rate of 1 billion waste tires per year (Hailstone 2022). The accumulation of waste tires in landfills can lead to the release of harmful chemicals into the environment, including methane gas, which contributes to the greenhouse effect. Additionally, if these tires catch fire, they can release toxic smoke into the atmosphere (ECOGREEN 2021). The

✉ Arash Akbari Hamed
akbarihamed.a@sut.ac.ir

[1] Faculty of Civil Engineering, Sahand University of Technology, Tabriz, Iran

Published online: 06 February 2024

production of new tires and the retreading process also contribute to carbon emissions, with 31 kg and 22 kg of CO_2 produced, respectively (VehicleServicePros 2020). To combat the negative effects of climate change and achieve net zero carbon emissions, it is crucial to prioritize the use of non-biodegradable waste materials. One promising solution is to repurpose scrap tires to create cost-effective and sustainable seismic base isolators, which can help reduce the environmental impact of construction and minimize damage from natural disasters in rural areas and low-rise buildings.

Kelly (Kelly 2002) conducted experimental tests on a low-cost strip isolator that was reinforced with carbon fiber. The purpose of this study was to develop a solution for the developing world, and the vertical stiffness of the isolator was evaluated theoretically based on the flexibility of reinforcement and the compressibility of elastomer. In addition, the use of low-cost scrap tire pads with different properties was investigated as seismic base isolation by (Özden 2006; Turer and Özden 2008). The performance of these pads was successfully evaluated through axial compression and shear tests. The researchers concluded that the shear stiffness of scrap tire pads could be adjusted by changing the number of tire layers, and their size could be altered by placing side-by-side longer strips or by using a woven structure. Konstantinidis and Kelly examined two types of low-cost seismic isolation systems, which replaced thick and inflexible reinforcing steel plate elements with thin flexible reinforcements such as carbon fibers and steel shims. Both theoretical and experimental tests were conducted on these systems (Konstantinidis and Kelly 2012, 2014). From 2012 to 2014, an extensive investigation into the performance of unbonded and bonded scrap tire rubber pads (STRP) through numerical simulations and experimental analysis was done by Mishra et al. (Mishra 2012; Mishra and Igarashi 2012; Mishra et al. 2012, 2013, 2014). The findings of these studies indicated that these cost-effective base isolators exhibit comparable axial pressure tolerance to conventional bearings, effectively reducing structural responses to acceptable levels during seismic events. Furthermore, the researchers concluded that both unbonded and bonded STRPs can be considered as viable seismic isolation devices for structures. In addition, Wand and Zhang conducted a study in which they designed 90 STRPs with varying geometric parameters, tire types, and loading conditions. Their investigation focused on evaluating the impact of these factors on the damping ratio, vertical and horizontal stiffness of the STRPs. The results of their study demonstrated that structures equipped with these low-cost base isolators can effectively reduce peak floor accelerations by up to 56.64% when compared to fixed-base structures (Wang and Zhang 2023).

Extensive and valuable research conducted by various researchers has led to a significant improvement in the performance of low-cost base isolators. As a result, it has been observed that the use of STRPs presents a viable and sustainable solution for protecting rural and low-rise buildings. The objective of this study is to examine the seismic performance of six new types of STRPs. These include: (1) STRP with unbonded rubber layers, (2) STRP with bonded rubber layers, (3) STRP with bonded rubber layers and loading steel plates, (4) STRP with bonded rubber layers and steel layers, (5) STRP with bonded rubber layers and lead core, and (6) STRP with bonded rubber layers and vertical steel rods. In order to achieve this objective, the finite element modeling procedure was validated, and the considered STRP base isolators were modeled. Their compression and shear behavior were then evaluated numerically. Finally, the seismic behavior of fixed-base and base-isolated two-story steel building models was investigated using the selected earthquake accelerograms.

2 The Concept of STRP Base Isolators

The STRP base isolators are constructed using the thread section of discarded tires that are sliced into smaller rectangular strips and then layered on top of each other. The inclusion of reinforcing steel cord layers, such as the belt and carcass layers, provides the necessary vertical rigidity to the STRP and prevents any lateral bulging of this economical bearing. Regarding Mishra (2012), the unbonded STRPs were constructed using six layers in which each layer consisted of five steel reinforcing cords. The considered material properties for the shear modulus of tire rubber (G), Poisson's ratio of steel reinforcing cords (υ), and Young's modulus of steel reinforcing cords (E) were 0.89 MPa, 0.3, and 200 GPa, respectively. The square-shaped STRPs had a width of 100 mm and a total thickness of 72 mm. Each layer had a thickness of 12 mm, while each steel reinforcing cord had a thickness of 0.4 mm. Consequently, the net total thickness of rubber in the STRPs was calculated to be 60 mm.

3 Verification of Finite Element Modeling Method

In order to validate the finite element modeling procedure, the six-layer unbonded STRP specimen (Mishra 2012) was modeled. The solid elements were used to model the rubber layers and upper and lower steel loading plates, while surface elements were utilized to model the reinforcing steel cord layers embedded in tire rubbers, as depicted in Fig. 1a. The orientation angle of wires in the lowest carcass layer was assumed to be zero with respect to the horizon, whereas the orientation angle in the upper layers (i.e., belt layers) was considered to be $\pm 70^\circ$ with the wire spacing of 0.4 mm and the cross-section area of each single wire of 0.1256 mm^2.

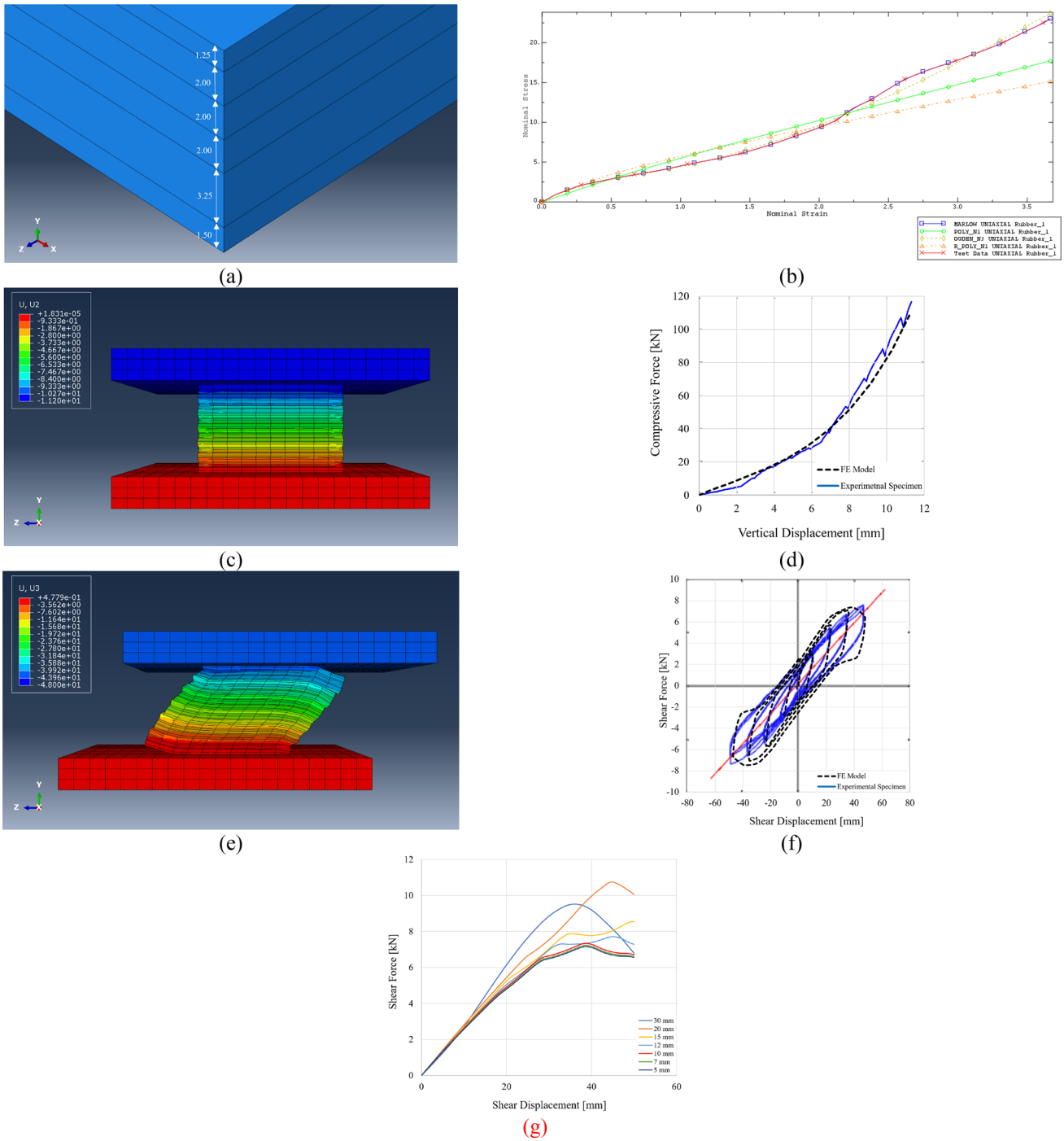

Fig. 1 **a** Position of the reinforcing steel cord layers inside each rubber layer (dimensions are in mm.), **b** comparison of rubber stress–strain curves obtained for the considered various strain energy potential models, **c** deformed shape of the six-layer unbonded STRP model at a vertical displacement of 11.2 mm, **d** comparison of the numerical and experimental hysteretic curves of the six-layer unbonded STRP model for the compression test, **e** deformed shape of the six-layer unbonded STRP model at a shear displacement of 48 mm, **f** comparison of the numerical and experimental hysteretic curves of the six-layer unbonded STRP model for the cyclic shear test, **g** mesh sensitivity analysis for the verified six-layer unbonded STRP model

It is worth mentioning that the different orientation angles lead to the anisotropic nonlinear behavior of tires. After evaluating various strain energy potential models for the hyperelastic material, it was concluded that the Marlow model provided the best match with the existing uniaxial test data (Fig. 1b); therefore, the Marlow hyperelastic material

with a near-incompressible Poisson's ratio of 0.45, along with the hysteresis behavior consisting of stress scaling factor = 1.6, creep parameter = 5, E_{ff} stress exponent = 4, and creep strain exponent = -1, was assigned to the tire rubber (Bergström and Boyce 1998). The penalty friction formulation was used to define the tangential behavior of contact property, with a friction coefficient of 0.95 and 0.8 between the rubber–rubber and rubber–steel layers, respectively. The hard contact normal behavior was assigned for the interaction between layers. Furthermore, the linear elastic isotropic behavior of steel material and the other dimensions of model were considered as mentioned in Sect. 2. Subsequently, the model was analyzed twice using the displacement-control general static procedure considering the geometrical nonlinearity to simulate the compression and cyclic shear tests performed by (Mishra 2012). It is worth noting that during the compressive test, the model was incrementally compressed until it reached a vertical displacement of 11.2 mm. As for the cyclic shear test, the model experienced incremental cyclic shear displacements with three repetitive cycles at each step. These displacements had amplitudes of 12 mm, 24 mm, 36 mm, and 48 mm. Additionally, an initial constant compressive load of 5 MPa was applied to the model. The deformed shape and force–displacement curves of the finite element model are depicted in Fig. 1c-f. The close resemblance between the numerical and experimental curves in this figure confirms the accuracy of the modeling procedure employed in this study. Figure 1g illustrates the pushover curves acquired for the six-layer unbonded STRP model, employing various mesh sizes to ascertain the optimal mesh size, which is determined to be 10 mm.

4 The Considered Sustainable and Economic STRP Base Isolators

In this section, the seismic performance of existing STRP isolators with unbonded and bonded rubber layers is compared to newly introduced STRP isolators. The new isolators include four variations: (1) STRP with bonded rubber layers and loading steel plates, (2) STRP with bonded rubber layers and steel layers, (3) STRP with bonded rubber layers and lead core, and (4) STRP with bonded rubber layers and vertical steel rods. All the considered STRP models in this study had a width of 100 mm and a total thickness of 72 mm, with each rubber layer having a thickness of 12 mm. The aspect ratio and shape factor, which are important factors in determining stability, shear deformation capacity, and stress demand of the STRP isolators, were kept constant at values of 1.389 and 2.083, respectively, for all models. As the seismic base isolators are typically utilized in axial pressure levels between 5 and 7 MPa (Kelly 1993a, b), all of them were examined under the simultaneous application of a constant compressive axial pressure of 6 MPa and incremental cyclic shear displacement. The shear displacement amplitudes include 12 mm, 24 mm, 36 mm, 48 mm, and 60 mm. In line with Mishra's research on unbonded STRP bearings (Mishra 2012), the maximum shear strain value was considered to be 83.33% for all the investigated models. By maintaining consistent conditions throughout the study, a fair comparison of the seismic performance of the different STRP isolators was achieved. It is worth noting that the geometrical and material properties of the STRP models, as well as their finite element modeling procedure, were consistent with those outlined in Sects. 2 and 3. It is noteworthy that in this study, various mesh elements were utilized for modeling purposes. For steel cord layers, linear quadrilateral elements of type SFM3D4 (i.e., four-node quadrilateral surface element) were used. Linear hexahedral elements of type C3D8R (i.e., eight-node linear brick, reduced integration, hourglass control) were employed for modeling steel and rubber plates. For steel rods, linear hexahedral elements of type C3D8R and linear wedge elements of type C3D6 (i.e., six-node linear triangular prism) were used. Bowl-shaped components were modeled using linear hexahedral elements of type C3D8R and quadratic tetrahedral elements of type C3D10 (i.e., ten-node quadratic tetrahedron). The lead core was modeled using linear hexahedral elements of type C3D8R. Different mesh techniques were used for different geometries in this study. Structured technique was used for regular geometries such as steel and rubber plates and steel cord layers. Sweep technique was employed for modeling the lead core, the plates with a central hole, and steel rods. Structured and free techniques were used for modeling the bowl-shaped components. The mesh sizes used in this study varied depending on the geometry being modeled. A mesh size of 10 mm was used for steel cord layers, steel and rubber plates. For steel rods, a mesh size of 5 mm was used. Bowl-shaped components and lead core were modeled using a mesh size of 3 mm. The deformed shape and hysteretic curves of the STRP models with unbonded and bonded rubber layers are depicted in Fig. 2a and b. The adhesive between the rubber layers was modeled using the Tie interaction, and the negligible thickness of the adhesive layers was disregarded to maintain the height of all compared models constant. The application of adhesive between rubber layers in STRP-2 resulted in the layers being held tightly without any slippage between them, unlike in STRP-1. However, both the unbonded and bonded STRPs exhibited similar shear force–shear displacement curves. In STRP-1 and STRP-2, there was no adhesive between the end rubber layers and upper and lower steel plates, leading to roll-off and the generation of large compressive stresses at two contacted corners, with no tension at the separated corners. As the resultant compressive force couple in elastomeric bearings balances the induced moment by the shear force, the

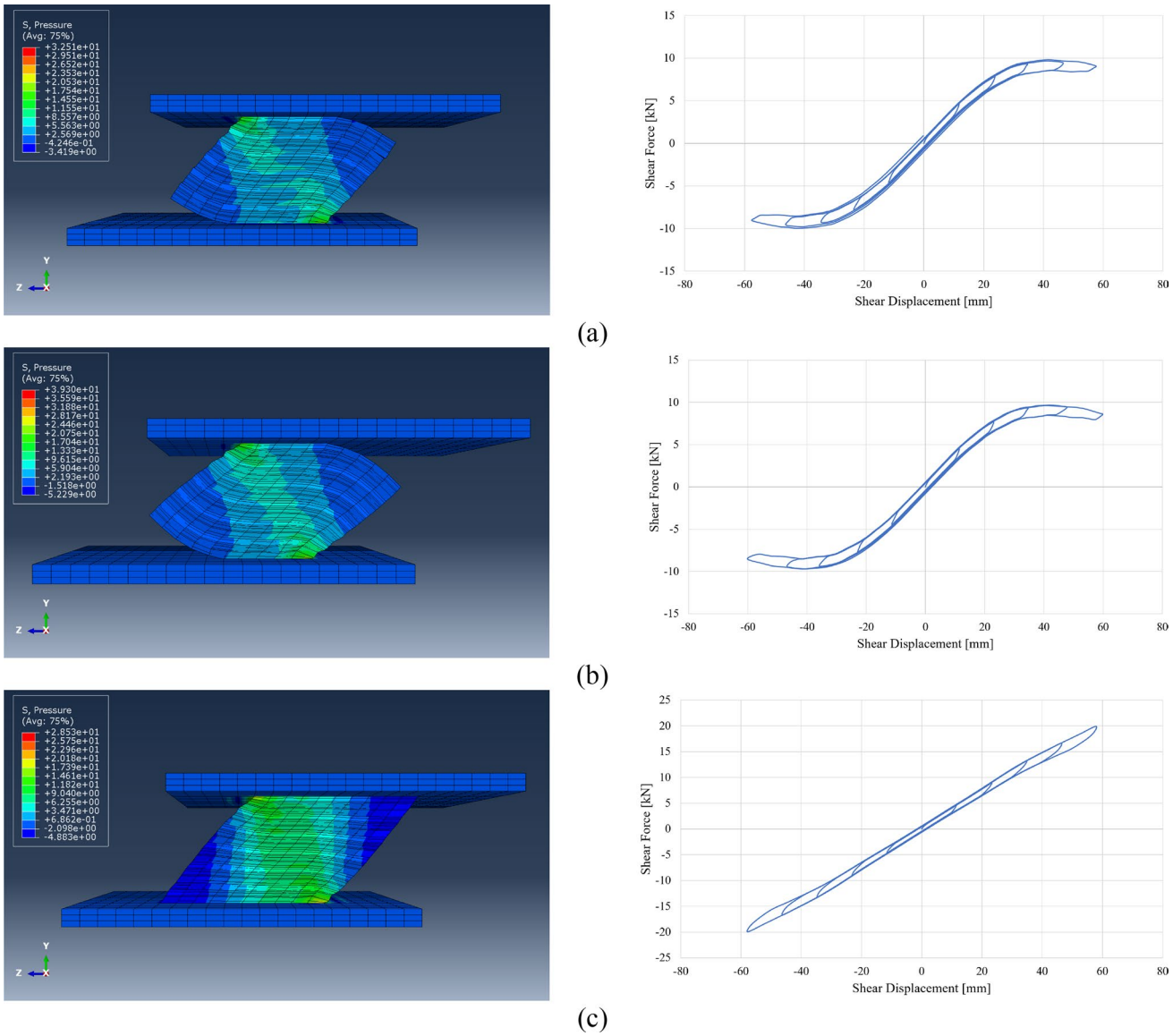

Fig. 2 Deformed shape and the force–displacement hysteretic curves of the STRP: **a** with unbonded rubber layers (STRP-1), **b** with bonded rubber layers (STRP-2), **c** with bonded rubber layers and loading steel plates (STRP-3)

shear resistance was reduced due to the roll-off, resulting in strength degradation in both bonded and unbonded STRPs at the shear displacement of 40 mm, equivalent to the shear strain of 55.56%. To address this issue, the STRP-3 model was introduced and examined in this study. This model involved bonding the end rubber layers to both the upper and lower steel loading plates, as illustrated in Fig. 2c. As can be observed from Fig. 2c, the reduction in contact area caused by the roll-out instability was eliminated, resulting in a uniformly distributed compression column zone from the top to the bottom of the STRP. Furthermore, the model was able to withstand tension stresses at the corners of the bearing, leading to an increase in its stability. As a result, a stable hysteretic shear force–shear displacement curve was achieved, and the shear strength of the STRP-3 was doubled. Additionally, the model was able to provide a shear deformation capacity of 83.33% (i.e., up to the end of applied loading) without significant strength or stiffness degradation.

Regarding Fig. 2, it is evident that although STRP-3 provides a stable hysteretic curve, there is an urgent requirement to enhance the seismic performance of STRPs in order to achieve greater seismic energy dissipation. In the case of unbonded STRPs, the input seismic energy is dissipated through three mechanisms: (1) friction between the rubber layers that causes slippage, (2) inherent damping of the rubber layers, and (3) friction generated between the individual filaments of the steel reinforcing cords when the cords are stretched due to induced shear deformation, resulting in

curved cross sections. Since the slippage between layers has been eliminated in STRP-3, additional elements need to be incorporated to achieve a more pronounced hysteretic curve. To address this objective, as illustrated in Fig. 3, three new STRP models were introduced and investigated in this study: (1) STRP-4 with bonded rubber and steel layers, (2) STRP-5 with bonded rubber layers and a lead core, and (3) STRP-6 with bonded rubber layers and vertical steel rods. In order to maintain a consistent overall height of 72 mm for all models, one of the rubber layers with a thickness of 12 mm was replaced with four steel layers, each with a thickness of 3 mm, in the STRP-4 model (Fig. 3a). In the case of STRP-5, a circular lead core with a diameter of 18 mm was positioned at the center of the stacked rubber layers (Fig. 3b). The material properties of lead considered in this study were as follows: Young's modulus = 16,000 MPa, Poisson' ratio = 0.42, and yield strength = 5.5 MPa. Figure 3c illustrates the placement of four steel circular rods at the corners

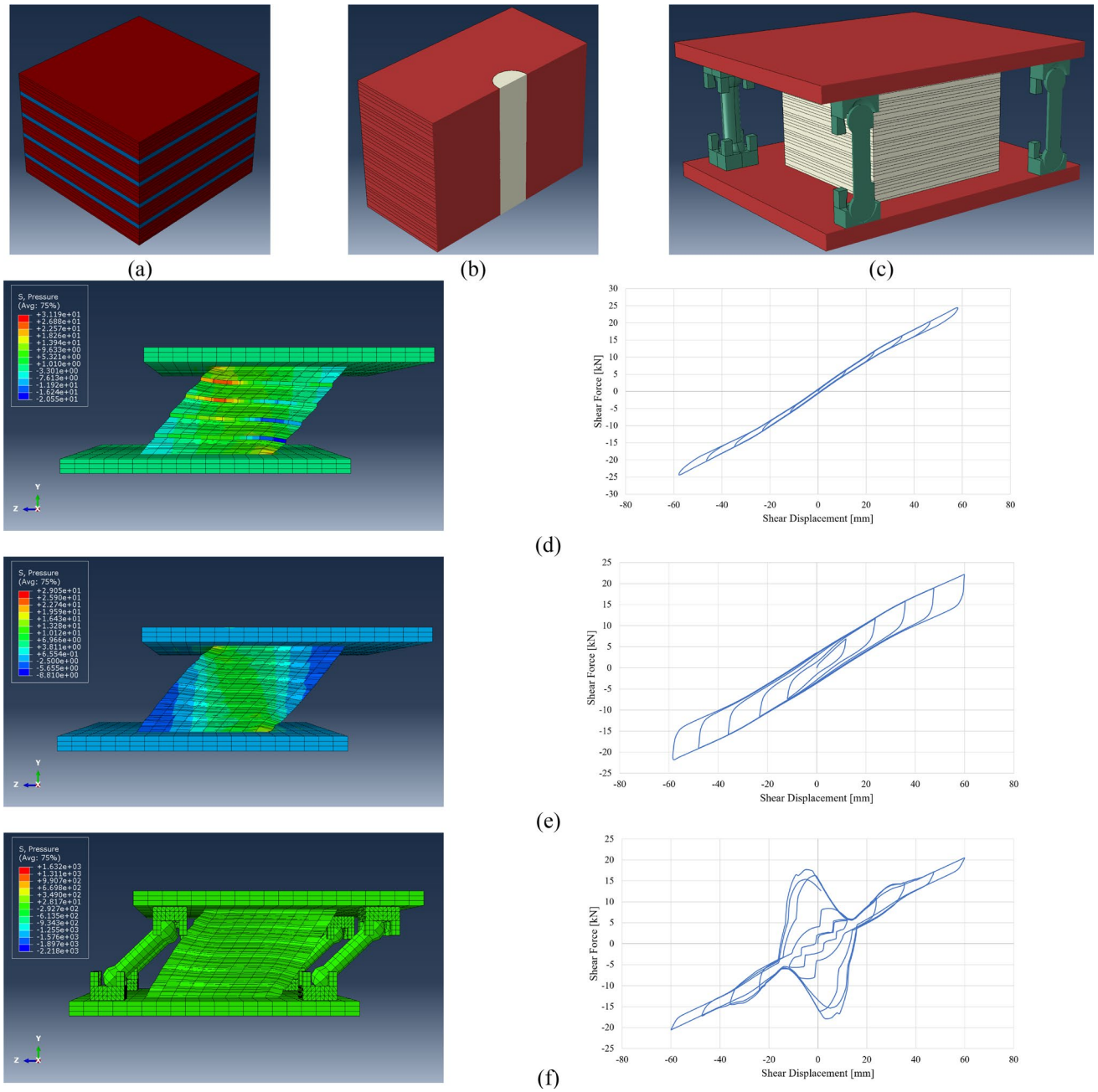

Fig. 3 The schematic view of the STRP: **a** with bonded rubber and steel layers (STRP-4), **b** with bonded rubber layers and lead core (STRP-5), **c** with bonded rubber layers and vertical steel rods (STRP-6), Deformed shape and the force–displacement hysteretic curves of **d** STRP-4, **e** STRP-5, **f** STRP-6

of the STRP-6. These rods are equipped with spherical parts at both ends, which are housed within bowl-shaped components. This design allows for easy movement of the rods during an earthquake, enabling them to dissipate seismic energy through friction. It is important to note that the friction coefficient between the steel rods in the STRP-6 is considered to be 0.5. Additionally, in all three STRP models (STRP-4, STRP-5, and STRP-6), the rubber layers and steel loading plates are bonded together, similar to STRP-3. Examining Fig. 3d, it is evident that the inclusion of steel plates in the STRP-4 results in a 25% increase in shear strength compared to STRP-3. However, despite the stable hysteretic curve without degradation, the enhancement in energy dissipation is not significant. On the other hand, Fig. 3e and f demonstrates that both STRP-5 and STRP-6 exhibit similar shear strength and shear deformation capacity while there is a substantial increase in the amount of dissipated energy. It is worth mentioning that the presence of a chubby part in the hysteretic curve of STRP-6 (Fig. 3f) can be attributed to the frictional action of the steel rods.

5 The Best STRP Base Isolator

Regarding the findings presented in Sect. 4 (Fig. 4a), it appears that STRP-5 and STRP-6 exhibited superior seismic performance compared to the other STRP models under consideration. However, in order to make an accurate decision on the selection of the most suitable STRP bearings, this section provides a quantitative comparison of several important parameters that were calculated for the examined models. First and foremost, it is important to note that the STRPs must fulfill certain fundamental requirements in order to be considered as suitable seismic base isolators for construction applications. These requirements include: (1) a certain level of horizontal stiffness, (2) significant vertical stiffness, (3) damping, and (4) endurance. In light of this, the effective horizontal stiffness (K_{eff}) of the considered STRP models was calculated using Eq. (1), taking into account the hysteretic curves depicted in Fig. 4a.

$$K_{\text{eff}} = \frac{F^{+} - F^{-}}{\Delta^{+} - \Delta^{-}} \tag{1}$$

where F^{+}, F^{-}, Δ^{+}, and Δ^{-} are the maximum values of the shear force and shear displacement at each step of the obtained hysteretic curves. Then, the effective damping parameter (β_{eff}) was estimated for all STRP models using Eq. (2).

$$\beta_{\text{eff}} = \frac{2}{\pi}\left[\frac{E_{\text{loop}}}{K_{\text{eff}}(|\Delta^{+}| + |\Delta^{-}|)^2}\right] \tag{2}$$

where E_{loop} is the amount of dissipated energy at each loading cycle. It is worth noting that the relationships presented in Eqs. (1) and (2) have gained widespread acceptance. These equations, proposed by UBC97 (UBC97 1997) and ASCE7-22 (ASCE7-22 2022), are utilized for the computation of the effective stiffness and effective damping of an isolator unit in seismically isolated structures, respectively. Furthermore, the STRP models were pushed down up to a vertical displacement of 10 mm in a displacement-control manner. The resulting compressive force–vertical displacement curves can be seen in Fig. 4b. It is important to note that STRP-6 was pushed down in two different types of downward displacement. In one case, its lateral sway was restricted, as indicated by the dashed black curve in Fig. 4b. In the other case, it was allowed to sway freely, represented by the solid black curve in Fig. 4b. Upon analyzing Fig. 4b, it is evident that when the rubber layers were compressed to a vertical displacement of 3.6 mm, the gap between the spherical parts at both ends of the steel rods and the inner surface of the bowl-shaped parts (as shown in Fig. 3c) was filled. Subsequently, the additional compressive force was absorbed through the combined action of the steel rods and

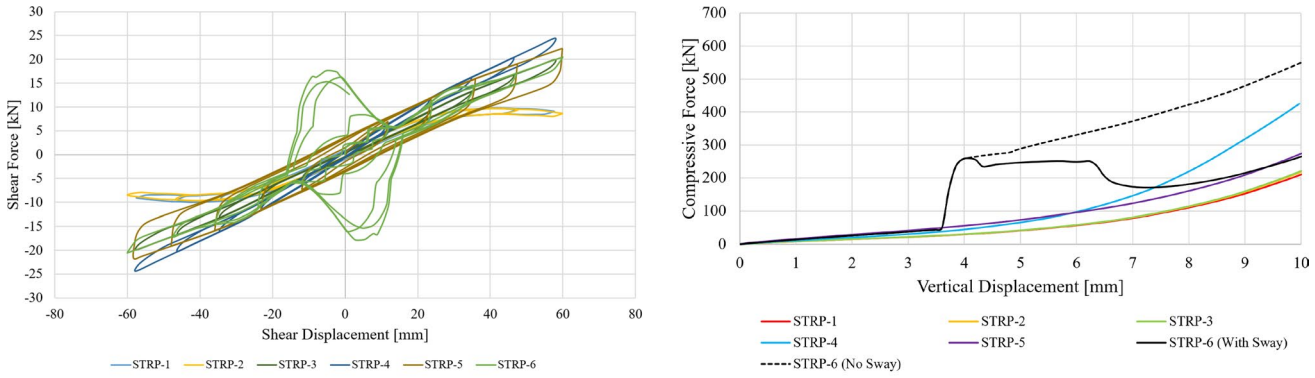

Fig. 4 Comparison of the shear force–shear displacement and compressive force–vertical displacement curves of the considered STRP models

rubber layers. When the upper steel plate was permitted to sway, a slippage plateau occurred. However, when the sway was restrained, the steel rods buckled upon reaching their critical compressive force.

Regarding Fig. 5a, which illustrates the K_{eff} values at different shear strains, it can be observed that STRP-1 and STRP-2 exhibited a significant decrease in effective horizontal stiffness due to roll-out instability. The rate at which K_{eff} approaches zero was faster for these models compared to the other STRP models. Consequently, STRP-1 and STRP-2 were unable to withstand higher horizontal forces at larger shear strains. Additionally, as the period of the base isolation system elongated, it was unable to provide the required horizontal frequency at higher shear strains. Furthermore, the ranking of the excellence in the variation of K_{eff} at different shear strain values is as follows: STRP-4, STRP-5, STRP-6, and STRP-3, respectively. Notably, STRP-3 maintained an approximately constant K_{eff} at various shear strains, while the K_{eff} values of STRP-3 and STRP-6 were equal after a shear strain of 67%. Considering Fig. 5b and c, it is evident that STRP-5 and STRP-6 ranked first in providing the initial and secant vertical stiffness, respectively. The vertical stiffness of bearings plays a crucial role in supporting vertical forces and minimizing the rocking motion of the isolated building. It is important to note that the calculation of the secant vertical stiffness was based on a line connecting the starting point of the compressive force–vertical displacement curves (Fig. 4b) to their endpoint at a vertical displacement of 10 mm. As shown in Fig. 5d and e, STRP-6 and STRP-5 ranked first and second, respectively, in terms of effective damping and total dissipated energy. Their β_{eff} values were higher than the 2–3% critical damping of natural rubber bearings (Naeim and Kelly 1999). It should be emphasized that the amount of dissipated energy and β_{eff}

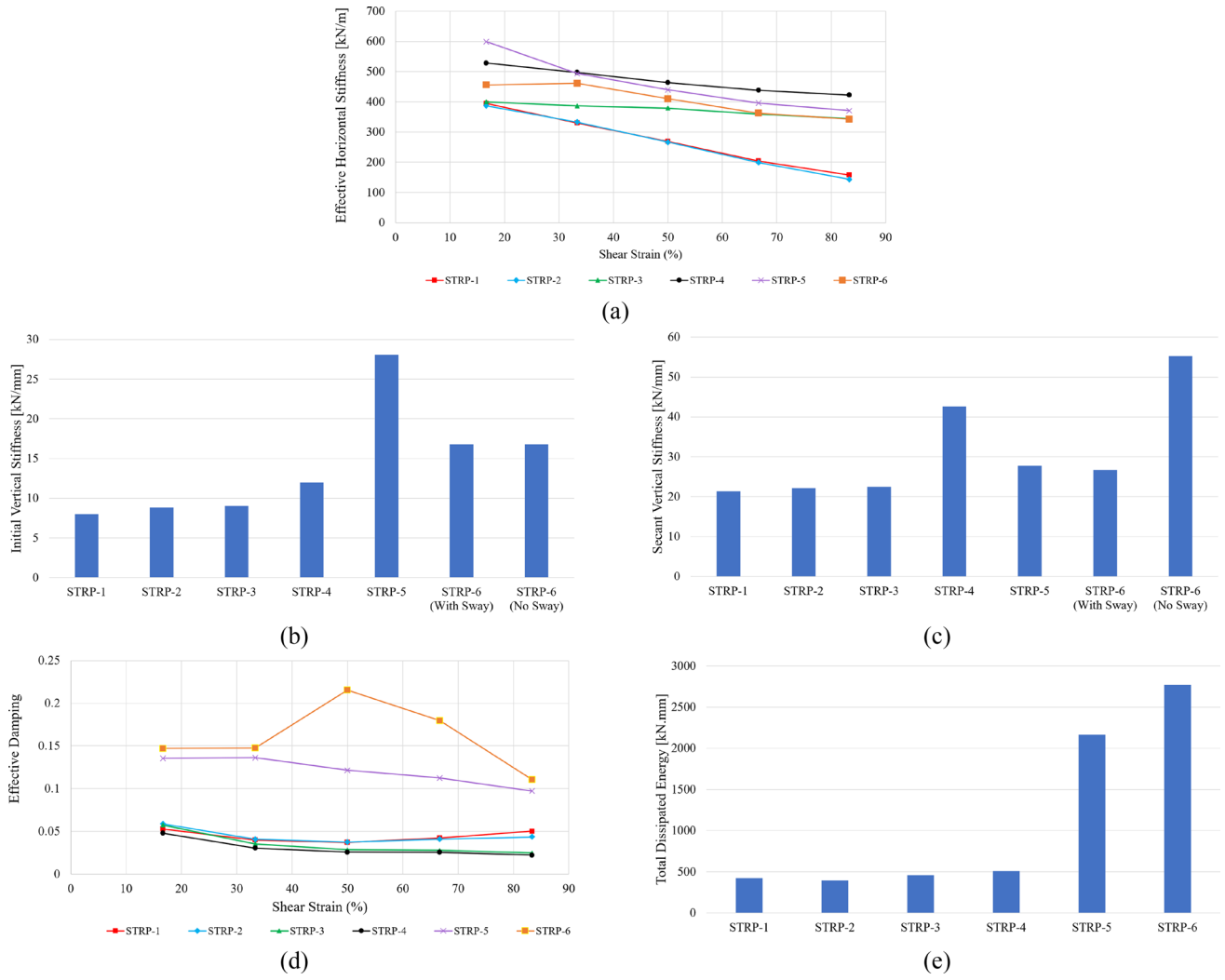

Fig. 5 Comparison of the performance of the considered STRP models based on: **a** effective horizontal stiffness, **b** initial vertical stiffness, **c** secant vertical stiffness, **d** effective damping, **e** total dissipated energy

are crucial parameters for controlling the shear displacement of bearings to meet the allowable lateral displacements specified in design codes. This, in turn, has an implicit effect on enhancing the endurance of bearings under cyclic loads. Overall, considering the results obtained for STRP-5 and STRP-6 in Sects. 4 and 5, such as the elimination of roll-out instability, the achievement of positive incremental and chubby shear force–shear displacement hysteretic curves up to a shear strain of 83.33%, the uniform distribution of compression column zone in the bearing, the average secant vertical stiffness to effective horizontal stiffness ratio of 60.53 for STRP-5 and 141.35 for STRP-6, the vertical secant stiffness of 55.25 kN/mm (which is sufficient for low-rise buildings), the average effective damping of 0.12 for STRP-5 and 0.16 for STRP-6, and the higher energy dissipation capacity of STRP-5 and STRP-6, it can be concluded that STRP-5 and STRP-6 are the most suitable STRP base isolators.

6 The Seismic Performance of low-rise Buildings Equipped with STRP Base Isolators

6.1 The Building Models and Considered Earthquake Records

In order to assess the seismic performance of buildings equipped with the most effective STRP base isolators under earthquake ground motions, a two-story building model with a three-span configuration was created. This model was designed to meet the requirements of a moderate ductility residential moment-resisting frame, situated in a high-seismicity region with stiff soil conditions. The floors and roof of the building were subjected to dead and live loads with intensities of 5.48 kN/m^2, 2 kN/m^2, 6.18 kN/m^2, and 1.50 kN/m^2, respectively. The fundamental period of the building model was determined to be 0.65 s, with a span length of 5 m and a story height of 3 m. The beams and columns were assigned steel sections of IPE300 and BOX180 × 180 × 20, respectively. To simplify the analysis process and save time, a nonlinear time history analysis of the building model was conducted using the dynamic implicit procedure, employing a two-degrees-of-freedom mass–spring–damper model. Considering that the dimensions of the investigated STRP models in previous sections were 100 × 100 × 72 mm, and the practical approximate dimensions of seismic elastomeric base isolators (i.e., prototype) are 750 × 750 × 540 mm, a scale factor of 7.5 (i.e., S = prototype/model = 7.5) was applied. This allowed for an accurate representation of the small-scale model in the analysis. The acceleration-based similitude law, as presented in Table 1 and proposed by (Kim et al. 2004), was utilized to ensure the fidelity of the scaled model. It is noteworthy that the fundamental periods for the prototype fixed-base, isolated with STRP-5 and STRP-6 building models were 0.65 s, 0.81 s, and 0.91 s, respectively. Additionally, the corresponding fundamental periods for the scaled fixed-base, isolated with STRP-5 and STRP-6 building models were 0.24 s, 0.30 s, and 0.33 s. These values align with the acceleration-based similitude law, as indicated by the scale factor for frequency in the last row of Table 1. It is important to highlight that STRP-5 and STRP-6, on average, enhance the value of the fundamental period by 32%, which is deemed satisfactory for this particular category of economic base isolators.

Table 1 Scale factors for the acceleration-based similitude law

Quantity	Dimension	Unit	Scale factor	Prototype	Model
Length	L	[mm]	S	–	–
Mass	M	[N.s^2/mm]	S^2	39.83	0.71
Time	T	[s]	$S^{1/2}$	–	–
Stress	$ML^{-1}T^{-2}$	[N/mm^2]	1	–	–
Velocity	LT^{-1}	[mm/s]	$S^{1/2}$	–	–
Acceleration	LT^{-2}	[mm/s^2]	1	–	–
Force	MLT^{-2}	[N]	S^2	–	–
Stiffness	MT^{-2}	[N/mm]	S	11,896.84	1586.25
Damping	MT^{-1}	[N.s/mm]	$S^{3/4}$	60.88	13.43
Frequency	T^{-1}	[1/s]	$S^{-1/2}$	–	–

A horizontal mass–spring–damper model was constructed in accordance with Fig. 6. This model consisted of two lumped masses that were interconnected and connected to the base through axial connectors. The properties of the axial connector were determined by analyzing the capacity curve (also known as the pushover curve) of each story in the designed building model, as illustrated in Fig. 7. Based on the scale factors provided in Table 1 and the capacity curve shown in Fig. 7, the elasticity behavior of the axial connector was assigned a value of 1586.25 N/mm (referred to as D11), while the plasticity behavior was defined by an uncoupled F1 with kinematic hardening using the half-cycle definition of force/S^2-plastic displacement/S. Additionally, a damping ratio of 0.05 led to the definition of the damping property of the axial connector as C11, with a value of 13.43 N.s/mm. The isotropic mass of 0.71 N.s2/mm was assigned to the reference points under consideration. Since the model was created in a horizontal position, the compressive effect of gravity loads on the base isolators was simulated by applying a concentrated force of 13,891.3 N (twice the weight of each lumped mass) to them. The entire model was then analyzed by applying earthquake accelerograms, with the total time and time steps scaled by a factor of 1/S$^{1/2}$. It is important to note that in the fixed-base model (Fig. 6a), all

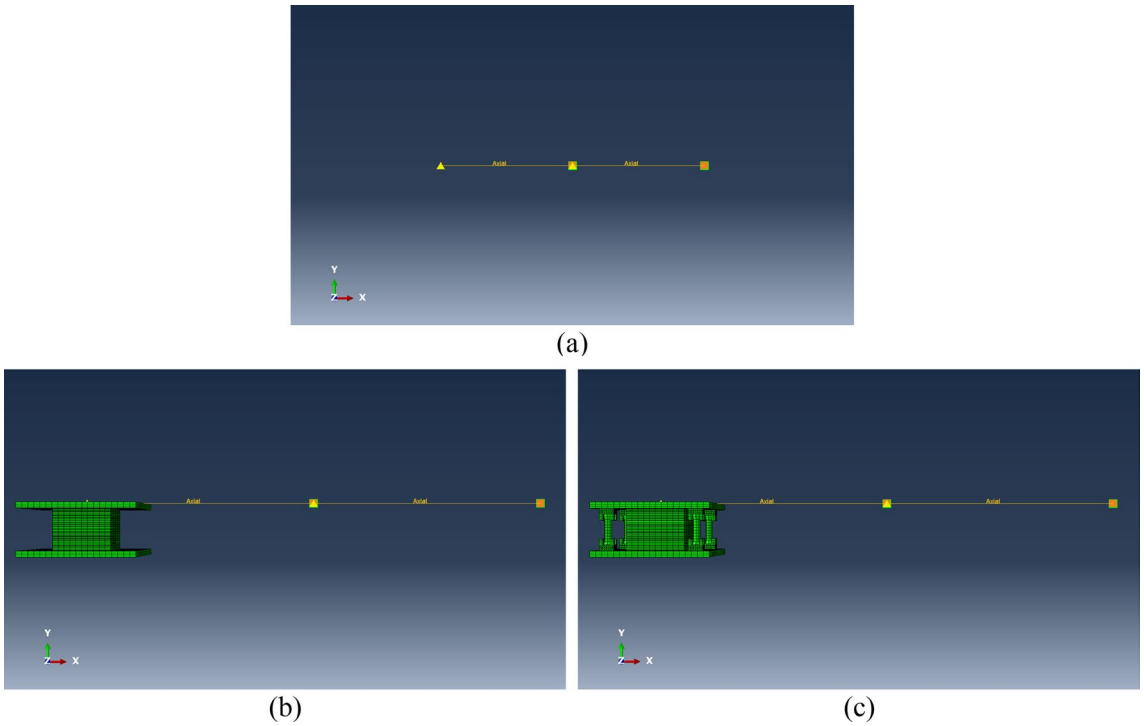

Fig. 6 The considered small scale mass–spring–damper building models with a: **a** fixed-base, **b** STRP-5, **c** STRP-6

degrees of freedom at the base and lumped masses were restrained, except for the translational degree of freedom in the *X* direction. In the base-isolated models (Fig. 6b and c), the assigned boundary conditions for the lumped masses were similar to those in the fixed-base model. However, at the location of STRPs, the translational degrees of freedom in the *X* and *Y* directions were free at the lower steel plate level, while the translational degree of freedom at the upper steel plate level was restrained.

In this study, eleven earthquake accelerograms were considered, each possessing the specific attributes outlined in Table 2. These records were scaled according to the provisions of Standard-2800 (Standard-2800 2014). The scale factors for each record were calculated and are displayed in Table 2. It is important to note that the far-field and near-field characteristics of the selected records, including the presence or absence of a pulse, were determined based on FEMA-P695. The scaled pseudo-spectral acceleration spectra for the earthquake records under consideration are depicted in Fig. 8.

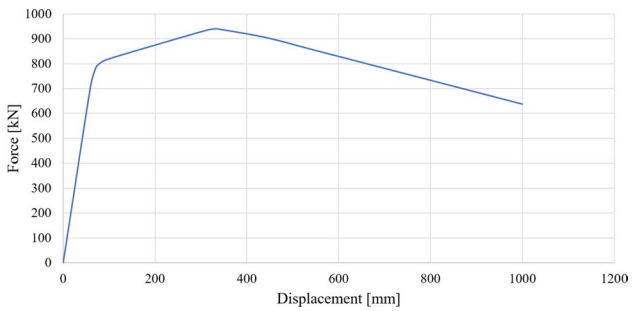

Fig. 7 Capacity curve of each story of the building model

6.2 Discussion on the Obtained Results

In Fig. 9, a comparison is presented between the absolute acceleration and interstory drift ratio time-histories for building models with fixed-base and those equipped with STRP-5 and STRP-6 bearings, subjected to earthquake ground motions. The results indicate that in fixed-base models, the absolute acceleration values for the second story were higher than those for the first story. However, when the building was equipped with STRP isolators, the absolute acceleration values were reduced and became approximately equal for both stories. Additionally, the interstory drift ratio for the first story was higher than that for the second story in both fixed-base and base-isolated buildings, but this was reduced by the application of STRP isolators. The results also show that the isolated buildings experienced a significant reduction in absolute acceleration and interstory drift ratio values compared to the fixed-base model during the Imperial Valley and Kobe earthquakes. Nevertheless, the decrease in structural responses was less pronounced

Table 2 The characteristics of considered earthquake records

Record Seq. No	Earthquake			Recording station name	PGA (g)	PGV (m/s)	Scale factor
	name	Year	M				
Far field record							
953	Northridge, USA	1994	6.7	Beverly Hills-Mulhol	0.52	0.63	0.968
1111	Kobe, Japan	1995	6.9	Nishi-Akashi	0.51	0.37	0.978
1633	Manjil, Iran	1990	7.4	Abbar	0.51	0.54	0.918
Pulse near field record							
292	Irpinia, Italy-01	1980	6.9	Sturno	0.31	0.455	1.474
821	Erzican, Turkey	1992	6.7	Erzican	0.49	0.955	0.952
1063	Northridge, USA	1994	6.7	Rinaldi Receiving Sta	0.87	1.673	0.541
1165	Kocaeli, Turkey	1999	7.5	Izmit	0.22	0.298	2.053
No pulse near field record							
160	Imperial Valley, USA	1979	6.5	Bonds Corner	0.76	0.443	0.789
741	Loma Prieta, USA	1989	6.9	Bran	0.64	0.559	0.941
1504	Chi-Chi, Taiwan	1999	7.6	TCU067	0.56	0.918	0.947
2114	Denali, Alaska	2002	7.9	TAPS Pump Sta. #10	0.33	1.264	1.421

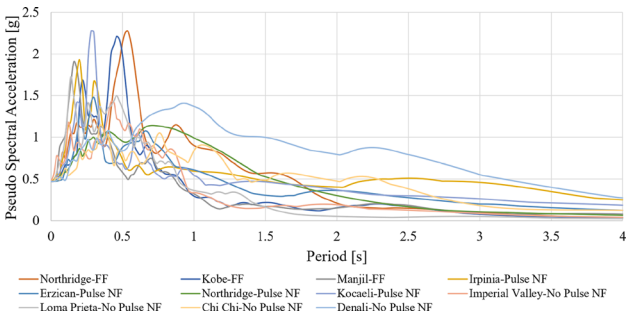

Fig. 8 The scaled pseudo-spectral acceleration spectra for the considered earthquake ground motions

during the Northridge earthquake. This can be attributed to the unique pulse near field characteristic of the Northridge record, as well as its significantly higher pseudo-spectral acceleration value at the fundamental periods of building models, when compared to Kobe and Imperial Valley records (Fig. 8). Notably, the interstory drift ratio time-histories in Fig. 9 indicate that the fixed-base model under Kobe and Northridge records experienced nonlinearity at the 1st story, resulting in residual drifts. This issue was eliminated by equipping the building model with STRP isolators, demonstrating the effectiveness of these bearings in protecting buildings against earthquakes.

Table 3 displays the results obtained from the building models' maximum absolute acceleration, maximum interstory drift ratio and maximum base shear under eleven different earthquake ground motions. The quantitative representation of the aforementioned conclusions from the previous paragraph can be observed in the difference percentage column of Table 3. It is evident that the building model subjected to the Northridge-Pulse NF and Denali-No Pulse NF records exhibited the most severe structural responses. Consequently, these cases demonstrated the least difference percentage values between the isolated models and the fixed-base models. In accordance with the Standard-2800 provisions, the average response among the eleven records should be considered. Therefore, based on the results obtained, the average difference percentages for the model with STRP-5 in reducing the maximum absolute acceleration, the maximum interstory drift ratio, and max. base shear were found to be 44.91%, 43.4%, and 54.24%, respectively. Furthermore, the average difference percentages for the model with STRP-6 in reducing the maximum absolute acceleration, the maximum interstory drift ratio, and max. base shear were determined to be 47.73%, 51.13%, and 59.27%, respectively. Figure 10 illustrates the contrast in the average reduction percentage of maximum absolute acceleration, maximum interstory drift ratio, and maximum base shear between the building models equipped with STRP-5 and STRP-6 and emphasizes the superior performance of the models incorporating STRP-6. In order to assess the overall effectiveness of the analyzed building models incorporating STRP-5 and STRP-6 when subjected to 11 different earthquake records, the seismic performance index (SPI) (Mualla and Belev 2002) was calculated using Eq. (3).

$$\mathrm{SPI} = \sqrt{R_d^2 + R_f^2 + R_e^2} \tag{3}$$

where R_d, R_f, and R_e are the displacement reduction factor, base shear reduction factor, and remaining energy factor, respectively. The estimated SPI values for the models incorporating STRP-5 and STRP-6 were 0.9 and 0.74,

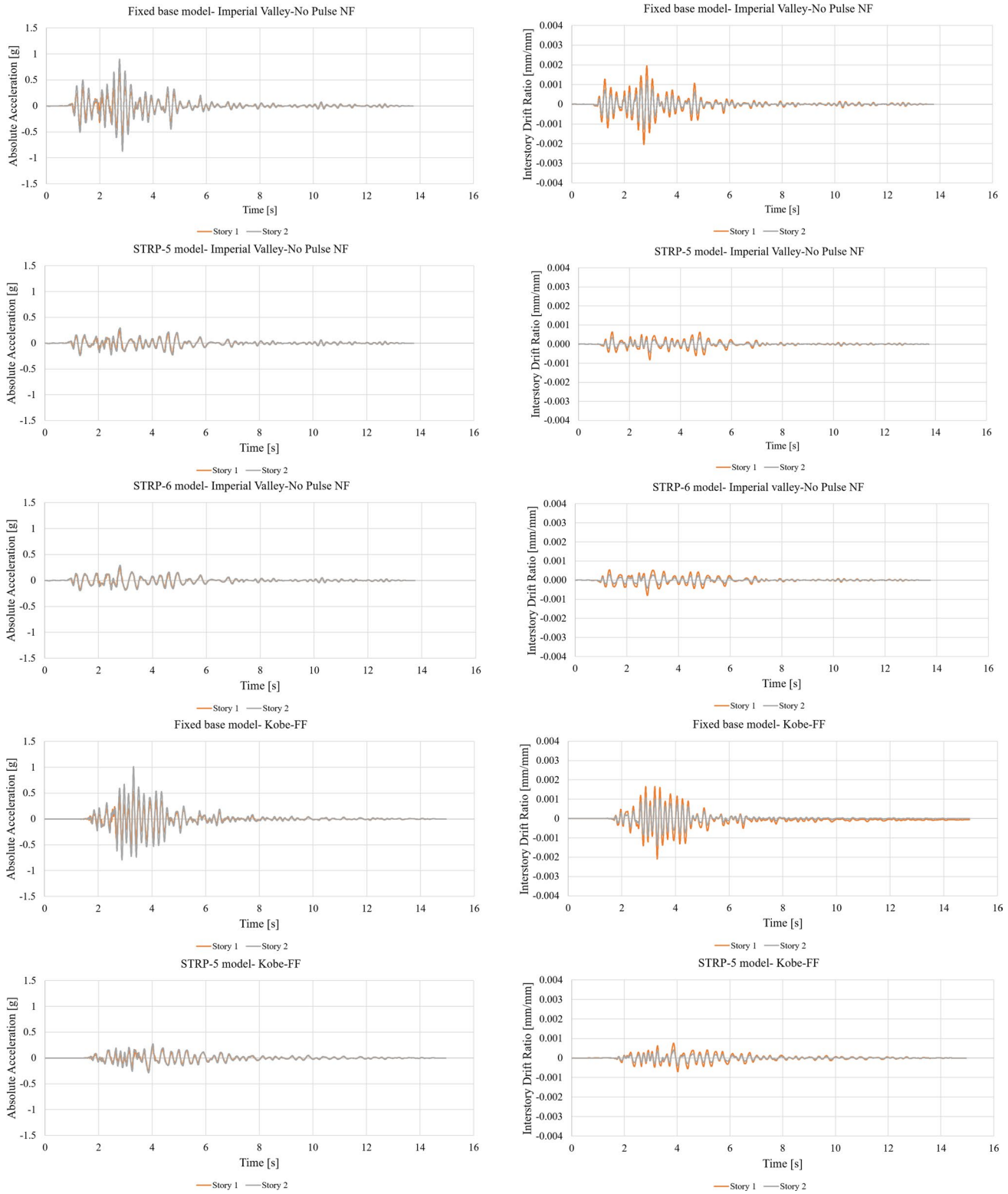

Fig. 9 Comparison of the absolute acceleration and interstory drift ratio time-histories for the building models with the fixed-base and equipped with STRP-5 and STRP-6 bearings under the considered earthquake ground motions

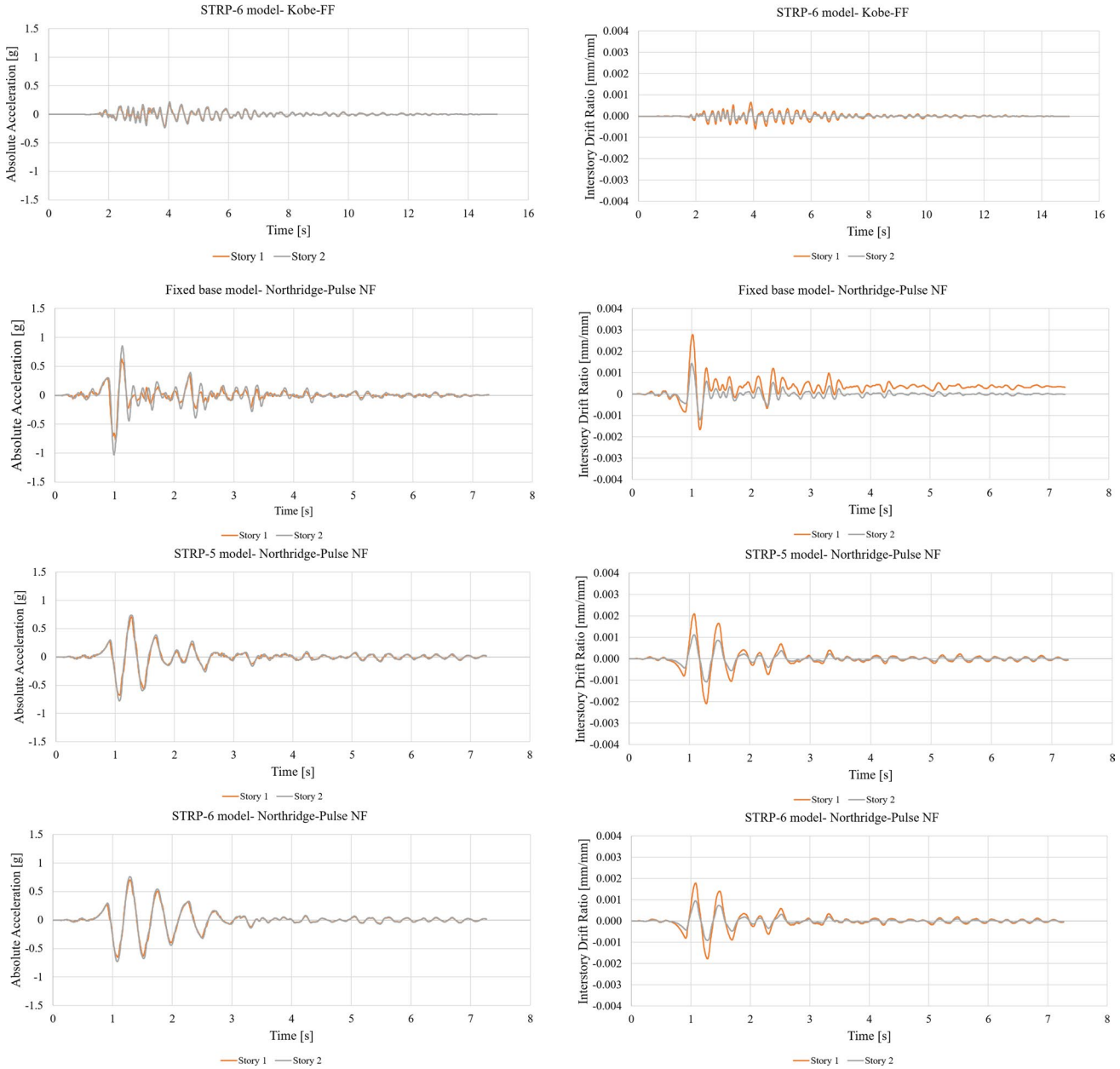

Fig. 9 (continued)

respectively. It is important to note that a lower value of SPI indicates a higher level of seismic isolation performance.

In light of the results obtained from Sects. 4 and 5, which demonstrate higher percentage values in reducing structural responses of buildings equipped with STRP-6 under the eleven considered ground motions, it has been confirmed that the novel STRP-6 isolator is efficient and superior in protecting low-rise buildings against far-field, pulse, and no pulse near-field earthquake records. This sustainable and economic base isolator, made with scrap tires, requires further investigation to assess its seismic performance in different low-rise structural systems equipped with STRP-6 isolator under more severe situations, such as mainshock-aftershock sequences (Basim et al. 2022), both numerically and experimentally.

7 Conclusions

In this research, a comprehensive investigation was conducted to evaluate the seismic performance of four novel types of sustainable and cost-effective base isolators, which were constructed using discarded tires. These isolators were compared with existing unbonded and bonded STRP

Table 3 The obtained values for max. absolute acceleration, max. interstory drift ratio, and max. base shear for the building models under 11 earthquake ground motions

Model	Earthquake record	Max. absolute acceleration		Difference percentage		Max. interstory drift ratio		Difference percentage		Max. base shear	Difference percentage
		[g]		[%]		[mm/mm]		[%]		[kN]	[%]
		Story 1	Story 2	Story 1	Story 2	Story 1	Story 2	Story 1	Story 2		
Fixed-base		Far-field record									
	Northridge	0.532	0.985	–	–	0.0021	0.0015	–	–	14.126	–
	Kobe	0.528	1.013	–	–	0.0021	0.0014	–	–	13.972	–
	Manjil	0.529	1.021			0.0023	0.0016			14.003	–
		Pulse near-field record									
	Irpinia	0.409	0.488	–	–	0.0013	0.0017	–	–	10.057	–
	Erzican	0.591	0.619	–	–	0.0019	0.0021	–	–	11.903	–
	Northridge	0.763	1.028	–	–	0.0028	0.0014	–	–	14.627	–
	Kocaeli	0.273	0.266	–	–	0.0007	0.001	–	–	7.774	–
		No pulse near-field record									
	Imperial Valley	0.62	0.902	–	–	0.002	0.0012	–	–	12.9	–
	Loma Prieta	0.57	0.811	–	–	0.0015	0.0009	–	–	11.305	–
	Chi–Chi	0.56	0.78	–	–	0.0014	0.0009	–	–	10.997	–
	Denali	0.71	1.101	–	–	0.0021	0.0013	–	–	14.02	–
Base isolated with STRP-5		Far-field record									
	Northridge	0.233	0.301	56.2	69.44	0.0009	0.0007	57.14	53.33	5.01	64.53
	Kobe	0.249	0.287	52.84	71.67	0.0008	0.0005	61.9	64.29	5.175	62.96
	Manjil	0.222	0.275	58.03	73.07	0.001	0.0009	56.52	43.75	4.801	65.71
		Pulse near-field record									
	Irpinia	0.312	0.338	23.72	30.74	0.0008	0.0006	38.46	64.71	4.01	60.13
	Erzican	0.503	0.439	14.89	29.08	0.0013	0.001	31.58	52.38	5.267	55.75
	Northridge	0.71	0.774	6.95	24.71	0.0021	0.0011	25	21.43	12.608	13.80
	Kocaeli	0.207	0.194	24.18	27.07	0.0005	0.0004	28.57	60	2.203	71.66
		No pulse near-field record									
	Imperial Valley	0.285	0.296	54.03	67.18	0.0009	0.0005	55	58.33	5.112	60.37
	Loma Prieta	0.213	0.218	62.63	73.12	0.0008	0.0007	46.67	22.22	4.144	63.34
	Chi-Chi	0.201	0.214	64.11	72.56	0.0008	0.0006	42.86	33.33	3.803	65.42
	Denali	0.664	0.821	6.48	25.43	0.0018	0.001	14.29	23.08	12.201	12.97

Table 3 (continued)

Model	Earthquake record	Max. absolute acceleration [g]		Difference percentage [%]		Max. interstory drift ratio [mm/mm]		Difference percentage [%]		Max. base shear [kN]	Difference percentage [%]
		Story 1	Story 2	Story 1	Story 2	Story 1	Story 2	Story 1	Story 2		
Base isolated with STRP-6		Far-field record									
	Northridge	0.217	0.229	59.21	76.75	0.0008	0.0007	61.9	53.33	4.102	70.96
	Kobe	0.202	0.233	61.74	77	0.0007	0.0004	66.67	71.43	4.004	71.34
	Manjil	0.22	0.248	58.41	75.71	0.0009	0.0008	60.87	50	4.266	69.54
		Pulse near-field record									
	Irpinia	0.302	0.331	26.16	32.17	0.0007	0.0005	46.15	70.59	3.51	65.10
	Erzican	0.482	0.409	18.44	33.93	0.001	0.0009	47.37	57.14	4.083	65.70
	Northridge	0.703	0.76	7.86	26.07	0.0018	0.001	35.71	28.57	11.991	18.02
	Kocaeli	0.189	0.179	30.77	32.71	0.0004	0.0003	42.86	70	1.907	75.47
		No pulse near-field record									
	Imperial Valley	0.271	0.293	56.29	67.52	0.0008	0.0004	60	66.67	4.942	61.69
	Loma Prieta	0.21	0.217	63.16	73.24	0.0007	0.0005	53.33	44.44	3.788	66.49
	Chi-Chi	0.196	0.207	65	73.46	0.0007	0.0006	50	33.33	3.016	72.57
	Denali	0.658	0.802	7.32	27.16	0.0016	0.0009	23.81	30.77	11.904	15.09

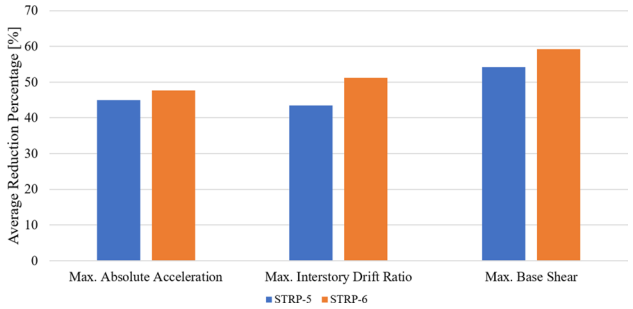

Fig. 10 Comparison of the average reduction percentage of max. absolute acceleration, max. interstory drift ratio, and max. base shear for the building models with STRP-5 and STRP-6

isolators. The study began by verifying the accuracy of the finite element modeling procedure. Subsequently, the monotonic compression and cyclic shear behavior of six different STRPs were examined. These included STRPs with unbonded rubber layers, bonded rubber layers, bonded rubber layers with loading steel plates, bonded rubber layers with steel layers, bonded rubber layers with lead core, and bonded rubber layers with vertical steel rods. The investigation focused on various important parameters, such as effective horizontal stiffness, vertical initial and secant stiffness, effective damping, total dissipated energy, and the overall shape of the obtained hysteretic curves. Based on these calculations, the most promising STRPs were identified. Furthermore, the seismic behavior of both fixed-base and base-isolated two-story steel building models was analyzed using earthquake accelerograms. The key findings of this study provide valuable insights into the effectiveness and suitability of the different STRPs for seismic isolation applications.

- STRP-1 and STRP-2 exhibited an incapacity to withstand amplified horizontal forces under greater shear strains. This can be attributed to their significantly declining effective horizontal stiffness, which was caused by roll-out instability. Moreover, Keff experienced a more rapid decrease, surpassing the rates observed in other STRP models.
- By implementing an adhesive layer between the rubber components and incorporating steel plates within the bonded STRPs, the issue of reduced contact area caused by roll-out instability was effectively resolved. This resulted in a uniform distribution of the compression column zone throughout the entire STRP, from its top to bottom. Consequently, the STRP-3 exhibited enhanced stability, enabling it to withstand tension stresses at the bearing's corners. As a result, a stable hysteretic shear force–shear displacement curve was achieved, leading to an increase in shear strength. Furthermore, the STRP-3 demonstrated a remarkable shear deformation capacity of 83.33%, allowing it to sustain applied loading until the very end without significant degradation in strength or stiffness.
- The inclusion of steel plates in STRP-4 resulted in a 25% increase in shear strength compared to STRP-3. However, despite maintaining a stable hysteretic curve without any degradation, there was not a significant increase in the amount of energy dissipation. On the other hand, both STRP-5 and STRP-6 exhibited similar shear strength and shear deformation capacity, but there was a notable increase in the amount of dissipated energy.
- It is noteworthy that previous research on STRPs has primarily focused on stacking multiple layers of scrap tires on top of each other, with the investigation of the use of adhesive between layers being the only aspect explored thus far. However, this study, as outlined in Sect. 4, delves into the analysis of previous models (STRP-1 and STRP-2) and initially investigates the use of adhesive between the upper and lower loading steel plates and rubber layers (STRP-3). This cost-effective base-isolator (STRP-3) exhibits improved behavior, including the elimination of strength and stiffness degradation, better stress distribution, and the elimination of roll-out instability. However, it requires greater energy dissipation. To address this issue, two models with the common concept of seismic base isolators, namely the use of steel layers (STRP-4) or a lead core (STRP-5), were generalized to STRPs and evaluated alongside a novel idea that had not been explored before (STRP-6). The new model (STRP-6) introduced in this study incorporates a friction damping mechanism, which is highly effective in dissipating seismic energy input. The inclusion of spherical surfaces within the bowl-shaped parts enhances the degree of freedom necessary for the base isolator to withstand earthquakes without compromising the flexibility of its rubber layers. The results indicate the superiority of the proposed model (STRP-6) over the lead core model (STRP-5), eliminating the need for lead and its detrimental effects on the environment as a toxic material. Furthermore, the proposed isolator (STRP-6) outperforms the conventional approach of using both steel and rubber layers simultaneously in base isolators (STRP-4). Based on the results obtained, it can be concluded that STRP-6 proved to be the most effective STRP isolator. This is evidenced by the elimination of roll-out instability, the achievement of positive incremental and chubby shear force–shear displacement hysteretic curves up to a shear strain of 83.33%, and the uniform distribution of compression column zone in the bearing. Additionally, the average secant vertical stiffness to the effective horizontal stiffness ratio of 141.35 and the vertical secant stiffness of 55.25 kN/mm were sufficient to carry the gravity loads in low-rise buildings and eliminate their rocking motion.

The average effective damping of 0.16 and higher energy dissipation capacity further support the effectiveness of STRP-6. Moreover, when compared to other models, the reduction of max. absolute acceleration, max. interstory drift ratio, and max. base shear were significantly higher with STRP-6, with average difference percentages of 47.73%, 51.13%, and 59.27%, respectively.

Acknowledgements This work is based upon research funded by Iran National Science Foundation (INSF) under project No. 4021667 which is gratefully acknowledged.

Author contributions Arash Akbari Hamed: Conceptualization, Methodology, Software, Validation, Formal analysis, Investigation, Resources, Data Curation, Writing - Original Draft, Writing - Review & Editing, Visualization, Supervision. Mahsa Saeidzadeh: Software, Validation, Formal analysis, Investigation, Resources, Data Curation, Writing - Original Draft, Writing - Review & Editing, Visualization. Hesam Bafandeh Nobari: Software, Investigation, Resources, Data Curation, Writing - Review & Editing. Farid Ostadhasanzadeh Maleky: Software, Validation, Formal analysis, Investigation, Resources, Data Curation.

Declarations

Conflict of Interest On behalf of all authors, the corresponding author states that there is no conflict of interest.

References

A Turer B Özden 2008 Seismic base isolation using low-cost scrap tire pads (STP) Mater Struct 41 891 908

A Akbari Hamed M Mofid 2015 On the plastic analysis of concentrically braced frames with shear panel, obtaining predetermined collapse mechanism Struct Des Tall Spec Build 24 5 366 395

A Akbari Hamed M Mofid 2017 Plastic design of eccentrically braced frames with shear panels Proc Inst Civ Eng-Struct Build 170 1 17 32

A Akbari Hamed SF Mortazavi M Saeidzadeh 2023 Evaluation of the seismic performance of structures equipped with novel multi-level TADAS dampers As J Civ Eng 24 4 969 988

A Akbari Hamed SS Hashemi 2023 Parametric study on the structural performance of ordinary, bamboo-shaped and triple-truss confined all-steel BRBs with a circular core cross-section As J Civ Eng 24 1 25

ASCE7-22 (2022). Minimum Design Loads and Associated Criteria for Buildings and Other Structures, American Society of Civil Engineers, Chicago

Basim MC., Pourreza F, Mousazadeh M, Hamed AA (2022). The effects of modeling uncertainties on the residual drift of steel structures under mainshock-aftershock sequences. Structures, Elsevier

ECOGREEN. (2021). Environmental impacts of waste tire disposal 2023, from https://ecogreenequipment.com/environmental-impacts-of-waste-tire-disposal/.

Hailstone, J. (2022). What happens when tires reach the end of the road?", 2023, from https://www.forbes.com/sites/brianbushard/2023/05/19/jetblue-american-airlines-partnership-rejected-judge-rules/?sh=57b4bca13d47.

Hamed AA, and Basim MC. (2020). Experimental-numerical study on weakened HSS-to-HSS connections using HBS and RBS approaches. Structures, Elsevier

AA Hamed A Samadi MC Basim 2022 Topology and shape optimization of steel plate shear walls for enhancing the seismic energy dissipation capacity J Build Eng 57 104828

JS Bergström M Boyce 1998 Constitutive modeling of the large strain time-dependent behavior of elastomers J Mech Phys Solids 46 5 931 954

JM Kelly 1993a Earthquake-resistant design with rubber Springer

JM Kelly 2002 Seismic isolation systems for developing countries Earthq Spectra 18 3 385 406

Kelly, J. M. (1993). State-of-the-art and state-of-the-practice in base isolation. Seminar on Seismic Isolation, passive energy dissipation and active control (ATC-17–1), Applied Technology Council, Redwood City.

Kim, N.-S., Y.-H. Kwak and S.-P. Chang (2004). Pseudodynamic tests on small-scale steel models using the modified similitude law. Proceedings of the 13th world conference on earthquake engineering.

Konstantinidis, D. and J. Kelly (2012). Two low-cost seismic isolation systems. 15th world conference on earthquake engineering. Lisbon, Portugal: September.

Konstantinidis, D. and J. Kelly (2014). Advances in low-cost seismic isolation with rubber. Proceedings of the 10th US National Conference in Earthquake Engineering.

HK Mishra A Igarashi 2012 Experimental and analytical study of scrap tire rubber pad for seismic isolation Int J Civ Environ Eng 6 2 107 113

HK Mishra A Igarashi H Matsushima 2013 Finite element analysis and experimental verification of the scrap tire rubber pad isolator Bull Earthq Eng 11 687 707

HK Mishra A Igarashi D Ji H Matsushima 2014 Pseudo-dynamic testing for seismic performance assessment of buildings with seismic isolation system using scrap tire rubber pad isolators J Civ Eng Archit 8 1 73

Mishra, H. K., A. Igarashi, H. Matsushima and A. Furukawa (2012). Experimental and analytical study of unbonded and bonded scrap tire rubber pad as base isolation device. 15th world conference on earthquake engineering, Lisbon, Portugal.

Mishra, H. K. (2012). Experimental and analytical studies on scrap tire rubber pads for application to seismic isolatiion of structures. PhD, PhD Dissertation, Kyoto University.

IH Mualla B Belev 2002 Performance of steel frames with a new friction damper device under earthquake excitation Eng Struct 24 3 365 371

F Naeim JM Kelly 1999 Design of seismic isolated structures: from theory to practice John Wiley & Sons

B Özden 2006 Low-cost seismic base isolation using scrap tire pads (STP) Middle East Technical University Ankara

M Saeidzadeh MR Chenaghlou AA Hamed 2022 Experimental and numerical study on the performance of a novel self-centering beam-column connection equipped with friction dampers J Build Eng 52 104338

Saeidzadeh, M., M. R. Chenaghlou and A. A. Hamed (2023). Mechanical model and seismic performance of frames with a self-centring connection. Proceedings of the Institution of Civil Engineers-Structures and Buildings. pp 1–16.

Standard-2800 (2014). Iranian seismic provisions standard. Road, Housing and Urban Development Research Center, Tehran

UBC97 (1997). Uniform Building Code- Volume 2. California, USA, International Conference of Building Officials.

VehicleServicePros. (2020). New study looks at carbon footprints of tires, retreads. 2023, from https://www.vehicleservicepros.com/shop-operations/collision-repair/business-and-finance/article/21171888/new-study-looks-at-carbon-footprints-of-tires-retreads.

M Wang G Zhang 2023 A low-cost isolator of scrap tire pads in rural construction: Evaluation of the mechanical properties and numerical assessment of the response control effects J Build Eng 67 105996

Zayas, V., S. Low and S. Mahin (1989). "Seismic isolation using the Friction Pendulum system."

Zayas, V., S. Low and S. Mahin (1989). Shake Table Testing of a Friction Pendulum Seismic Isolation System. Seismic Engineering: Research and Practice, ASCE.